# The Case for Measurement and Analysis of ESD Fields in Semiconductor Manufacturing

Timothy J. Maloney
*Center for Analytic Insights*
Palo Alto, CA USA
tjmaloney@sbcglobal.net

***Abstract*—A destructive Charged Device Model electrostatic discharge event can happen in semiconductor manufacturing and should be detectable from radiation that results from collapse of an electric dipole. The analytically describable radiation field pulse of CDM can be readily produced with a new instrument (CDM Event Simulator or CDMES) that creates dipole collapse at will. A coaxial monopole E-field antenna's transfer function gives the antenna signal in near-field, and experiments compare well with theory. These and other instruments for CDM ESD monitoring and process control are described in a newly-issued patent, reviewed here.**

***Keywords—electrostatic discharge (ESD), charged device model (CDM), step response, Laplace Transforms, semiconductor manufacturing, E-field antenna, ESD detectors***

## I. INTRODUCTION

A Charged Device Model (CDM) electrostatic discharge (ESD) stress results when a charged component creates equal and opposite mirror charge in a ground plane, followed by collapse of the electric dipole in a current pulse when the affected pin touches ground. In recent years, workers have sought to measure such ESD events or monitor them in the factory by detecting radiated fields with a nearby antenna [1-4]. This has achieved some static monitoring and control, but it has not been clear how to interpret the measured antenna waveforms in terms of the more familiar component CDM current waveforms and charge quantities. Also, factory tools are being outfitted with compact CDM ESD threshold detectors, fed by antennas situated near the possible source of ESD events. This motivates us to relate the yes/no thresholds of these electronic boxes, at a particular setting, to the expected properties of the antenna pulses coming in.

The author's 2011 paper [5] described, in analytic form for free space, the small collapsing dipole pulses common to CDM events. These are pulsed Hertzian dipoles, much as long described in the literature for pulsed transmitting antennas but using a unique pole-zero treatment that captures all near and far fields (static field, induction field, radiated field) at once. This formulation, using complex frequencies to describe the current and field pulses, allows inversion to the time domain through the inverse Laplace Transform, and thus provides us with the basic building blocks of the CDM fields. Then we need to find the expected response of an antenna to that field. Our example will be a simple E-field antenna with a straightforward transfer function for the expected signal into a 50 ohm scope. As seen in [3, 4], this pulse shape has been found to agree well with experiments, whereby an artificial CDM event produces a monitored current pulse and antenna signal simultaneously. The antenna is placed nearby (15 cm, for example), as it would typically be in factory equipment. Given the propagation time to the antenna location (500 psec) and the expected speed of the event (nanosecond or sub-nanosecond pulses, rise times down to 100 psec or less), both the near fields and far field contribute, but this is all captured in one pole-zero expression as in [5], employable in both time and frequency domains.

Once the overall behavior of antenna signals for CDM is described, computed, and measured, we need to measure the effect of such signals on whatever is used in manufacturing as a detector. This is likely to be a compact ESD detector box, a yes/no threshold detector, at a particular setting [3, 4]. Does triggering primarily depend on peak-to-peak voltage, as expected? What is the influence of pulse speed, and is signal dispersion in the cable important? For calibration purposes, the artificial air discharge CDM pulse and antenna can be replaced, in many respects, with a highly reproducible synthetic pulse that has much more dynamic range and is easier to use [3, 4]. Most elements of a manufacturing detection system, including a signal detector, were covered in a recently issued patent [6]. The basic factory setup from [6] is pictured in Appendix A, Fig. A1. Now that several years have passed since the initial studies and patent filing, it is useful to reflect critically on the elements of this ESD monitoring system, and discuss what kind of revisions and improvements are needed.

## II. PULSED FIELD THEORY AND PULSE GENERATORS

### *A. Pulsed Hertzian Dipole Field Theory*

Reference [5] is suitable for adopting its notation, coordinate system, field equations, and series RLC circuit models. Complex frequency $s=\sigma+j\omega$ will appear often. The focus of [5] is calculation of the pulsed electric dipole fields with extension to the complementary magnetic dipole as described therein. In [5], expressions for all electric dipole fields, near and far, electric and magnetic, radial, azimuthal and polar, are derived. We are primarily interested in the "equatorial" polar E-field $E_\theta$, aligned with the current source and electric dipole moment vector (z-direction), as this

induces the largest signal in the antenna (Fig. 1; also see Appendix A, Fig. A2). In the s-domain,

$$E_\theta(s) = \frac{I(s)\sin\theta}{4\pi\varepsilon_0 s r^3} dl \cdot (1 + s\tau + s^2\tau^2), \tau = \frac{r}{c}, \quad (1)$$

where the polar angle $\theta=\pi/2$ at the equator, r is the distance from the source, c is the speed of light, *dl* is the length of the dipole. As explained in [5], the three terms describe the static field, induction field, and radiation field in the complex frequency domain. We will describe the current pulse I(s) once we see an example of a current pulse produced by dipole collapse.

The E-field of an electric dipole is the only field to which our E-field antenna is sensitive; the polar field $E_\theta$ is the only E-field at the equator, as the radial field $E_r$ vanishes there. $E_r$ depends only on static and inductive terms. Meanwhile, the associated magnetic field $H_\phi$ is azimuthal and involves only the induction and far-field radiation terms. These facts are well established in standard textbooks [7, 8], but [5] offers a rare glimpse into the s-domain formulation (instead of setting $s=j\omega$) and thus allows direct access to the pulsed field solutions that we need for CDM.

### *B. CDM-like Pulse Source and Model*

A conceptual view of a generator of CDM-like pulses is shown in Fig. 2. A charged plate with a spring loaded pogo pin comes down on a pedestal at the end of the center conductor of a 50-ohm coax line with its shield on the ground plane. The field created between the charge plate and the ground plate then collapses and the current is detected by the 50-ohm scope connection. Note that any CDM spark resistance is in series with the 50 ohms, which raises the damping factor, simplifies the pulse, and makes ringing unlikely.

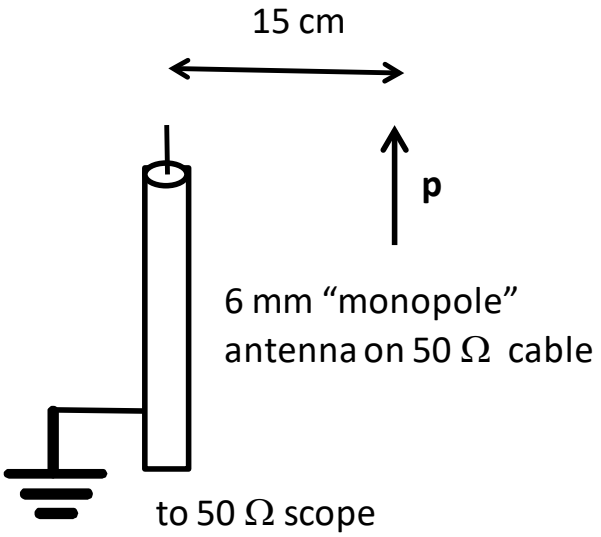


Fig. 1. Experimental arrangement of CDM electric dipole initial source **p** and 6 mm coaxial antenna.

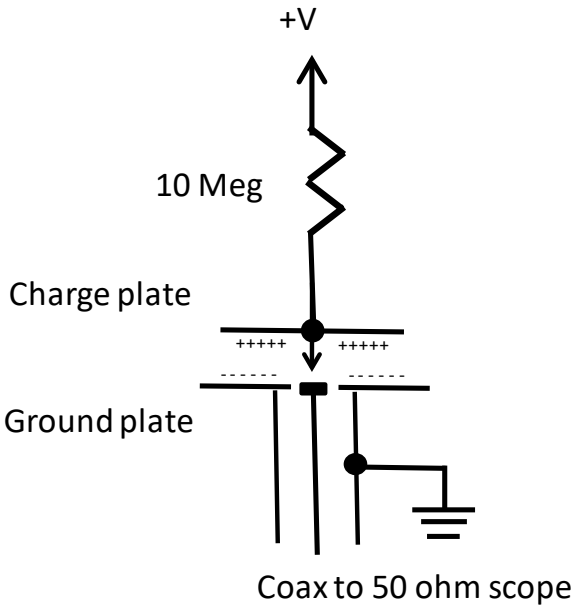


Fig. 2. CDM pulse generator. Charge plate probe hits pedestal and dipole collapses, with current pulse and dipole radiation.

The top trace in Fig. 3 shows the current pulse resulting from -100V applied to a pulse generator built as in Fig. 2, an instrument that has come to be known as the Charged Device Model Event Simulator (CDMES) [6]. A 3 GHz oscilloscope was used; the pulse has its peak and strongest derivatives in the first few hundred picoseconds.

We need a current function I(s) to approximate the pulse from this artificial CDM source. With a polynomial-based pole-zero expression, the fields can be computed using Heaviside inversion of the Laplace Transform [5]. The two-pole series RLC response to a step function is a favorite way to model a CDM pulse current [3-5, 9] that occurs through capacitive discharge such as in Fig. 2. This is even the case with human body model (HBM) currents [10]. One can avoid field singularities by putting enough polynomial order in the denominator of $E_\theta(s)$. We use high-speed poles to model a step source with finite rise time for the spark, and then multiply the familiar RLC expression for the rest of I(s) [5]. The author's publications from 2013-14 [9] show how to work from a CDM waveform to an equivalent RLC circuit with assigned element values.

There is a discussion of some length in Refs. [3, 4] that first formulates an analytic I(s) model of the current pulse of Fig. 3 and works toward a field solution, then an antenna response calculation. As we are space-limited in this work, we will cover the final results, and refer the reader to [3, 4] for the full discussion and other modeling considerations. These include poles to capture the 3 GHz oscilloscope filtering, in accordance with models in [11], and the use of Mathematica using Heaviside expansion to produce the inverse Laplace Transform for time domain response.

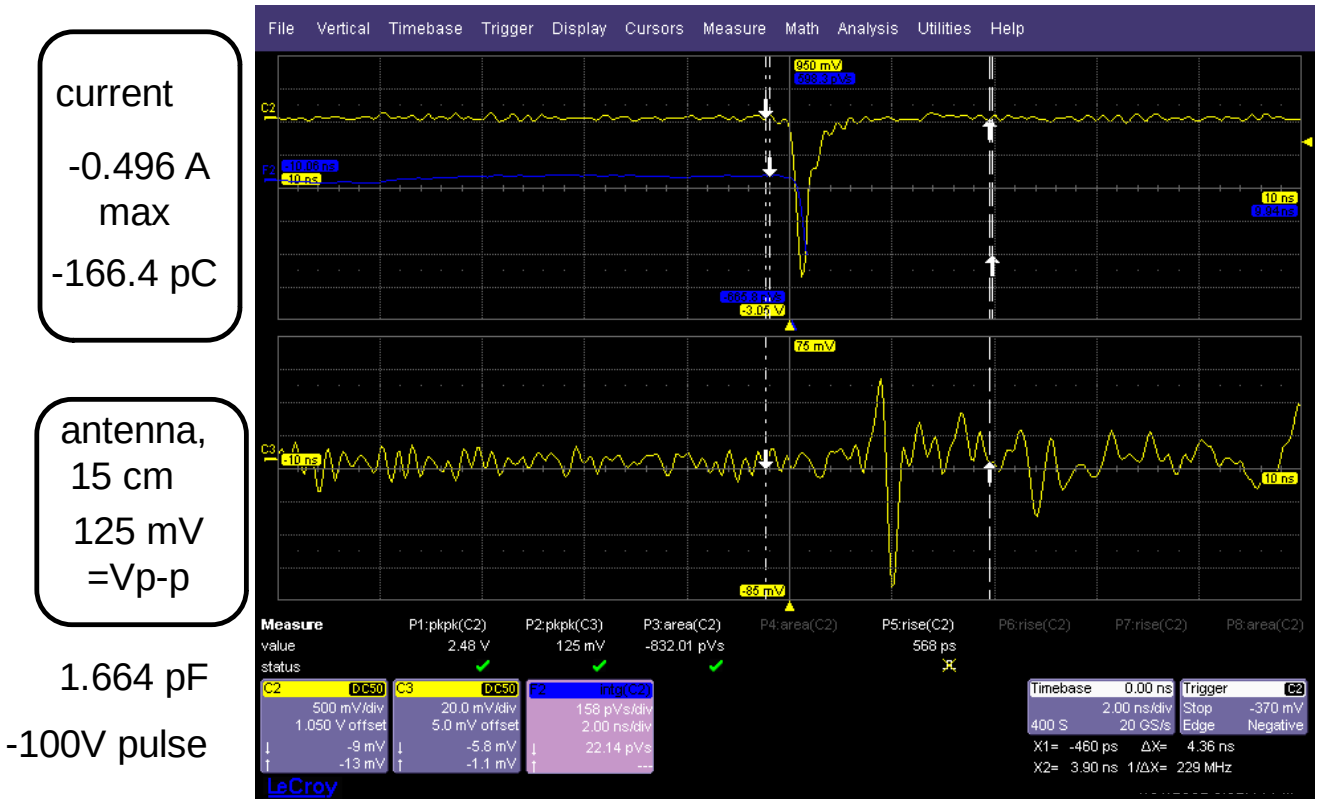


Fig. 3. Measured current (top) and antenna response (bottom) to E-field at 15 cm, using artificial CDM source; 2 nsec/division, 3 GHz scope. Setup as in Fig. 1, current polarity negative. Integrated current gives -166.4 pC of charge; 10x attenuation used.

## III. Calculated and Measured Antenna Pulses

The antenna used in these studies is a so-called monopole antenna made from coaxial cable. It is conceptually much as pictured in Fig. 1, aside from the Teflon cap over the 6 mm extension of the coaxial center conductor. A signal is generated as the E-field induces an electric dipole in the tip, driving the 50-ohm load. A simple circuit model gives the transfer function of such an antenna [12], and it can be applied as in [3-5] to give measured voltage $V_m$ as

$$\frac{V_m(s)}{E_{-z}(s)} = -\frac{l_m Z_0 C_m s}{1 + Z_0 C_m s + L_m C_m s^2}, \quad (2)$$

for which $Z_0$ is cable impedance (usually 50 ohms), $C_m$ and $L_m$ are the inductive and capacitive equivalents of the probe wire, and $l_m$ is the length of the probe wire. The field $E_{-z}=E_\theta$ when maximum at the equator, $\theta=\pi/2$, as before. The experimental setup, Fig. 1, defines positive polarity. To get the sign right, it is helpful to consider the initial induced dipole on the antenna; for a positive dipole as shown, there will be a net negative charge integrated from current during the collapse. The transfer function for our 6 mm probe is found from values suggested by [12], with $L_m$=5.1 nH and with a little more capacitance ($C_m$=0.38 pF) due to the Teflon cap. Combining (1) and (2), the "s" terms now cancel, so the signal will have no dc component, as expected, and will be influenced by the two new poles from the antenna, and we may see some ringing of the antenna itself. Filtering by the 3 GHz scope bandwidth [11] has been carried into the full transfer function as well. The attenuation of the coaxial cable (150 cm, RG-316) connection to the scope, due to skin effect and dielectric losses, are of some concern and can be calculated [13, 14]. These effects are estimated to be small enough to be absorbed by calibration, but before long a more detailed exact calculation of cable loss will be easier to perform [14].

Because the fields and final antenna signal are so sensitive to time derivatives as well dipole strength, the calculated antenna signal is very sensitive to the current function used to estimate it. After some tinkering [3, 4], the current function shown in Fig. 4a was found to work best for being transformed first into E-fields and then into an antenna signal. The calculated antenna signal in Fig. 4b corresponds well to Fig. 3 because the orientation of dipole and antenna is equal and opposite. Given the uncertainties and rough estimates of the model parameters of the antenna (particularly the effect of the antenna's Teflon cap) and the discharge source, plus slight differences each time for air spark, plus effects of stray fields from the chargeup wire (which were reduced through careful design but are hard to eliminate completely), the agreement between theory and experiment is quite good. It is a rare case of an *ab initio* pulsed field calculation followed by experiment. Such a crisp event as in Fig. 3 will not happen each time, but when it does, it is a worst case, and its maximum current, field, and antenna signal can be associated with a maximum likelihood of device destruction if detected in the factory.

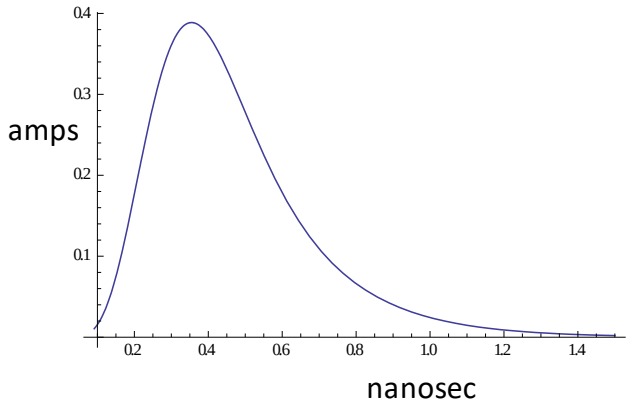


Fig. 4a. CDM current pulse that approximates current pulse measured in Fig. 3. 1.5 nsec full scale.

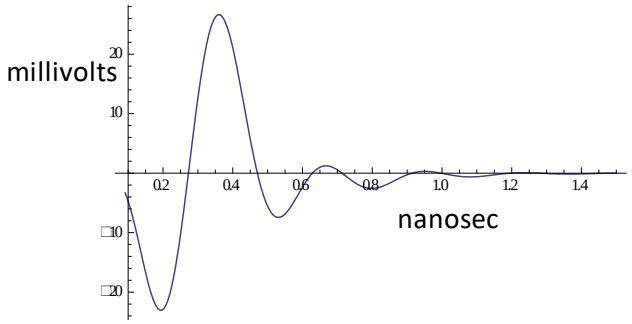


Fig. 4b. Calculated antenna response to E-field using current source of Fig. 4a. 15 cm from CDM source, 1.5 nsec full scale, 3 GHz scope filter. Alignment as in Fig. 1.

The main feature of the antenna pulse is the prominent "monocycle" pulse up front, present in Figs. 3-4, with its overall peak-to-peak voltage Vp-p found in the swing of the first two peaks. We suspect that most CDM ESD detectors will be sensitive to Vp-p. Refs. [3, 4] discussed, at some length, a method to generate monocycle pulses at the proper time scale, resembling Figs. 3 and 4b, in order to calibrate the detection system. The reader is referred to [3, 4] for details; we will use some of the results in the discussion that follows.

## IV. Discussion

### A. *Calibration of the ESD Detection System*

The monocycle pulse generator described in [3, 4] works by taking a transmission line pulse (TLP) step and differentiating it twice, using two quarter-wave directional couplers. The operative pulse comes from a 10X pickoff tee, so it has 450 ohm source impedance into a 50 ohm RG-316 cable—we will soon see why impedance is important. An example is shown in Fig. 5.

The monocycle pulser is intended for easy calibration of an ESD event detector that is otherwise intended to pick up pulses from a monopole antenna. To simulate the antenna source more fully, the pulse should originate from a high impedance source, as the monopole antenna is a DC open circuit. This was fully discussed in [3, 4]. The 450 ohm

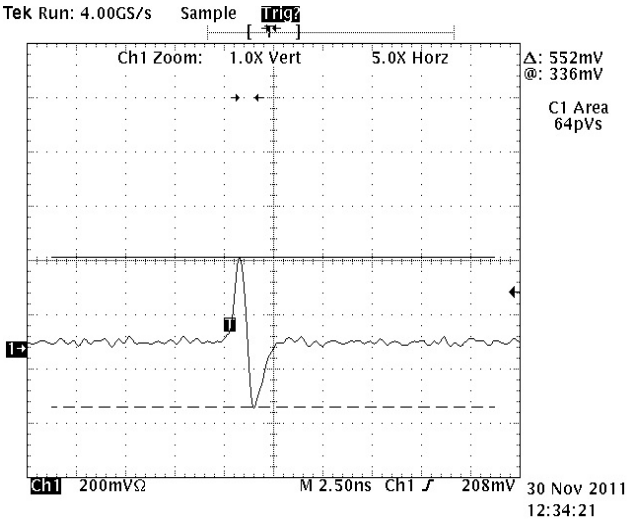


Fig. 5. Monocycle pulse output [3, 4]. Vp-p=552 mV after 10X attenuation. 1 GHz scope, 2.5 nsec/division.

output impedance of the pickoff tee will reflect nearly all of the signal reflected from the event detector, as would be the case with a monopole antenna. Also, the MiniPulse input to high-pass filters happens to have a strong reflection coefficient, so the cable is a resonant cavity.

The MiniPulse event detector [6] is set at an adjustable threshold sensitivity (1.2-1.9 volts) and initiates an alarm when an event is triggered. The setting relates to the output of internal high-pass filters and a logarithmic amplifier, allowing a large dynamic range of antenna signals. Thus we hoped that our simple metric of "Vp-p of a fast monocycle pulse" would relate in a meaningful way to the setting of the MiniPulse event detector. Indeed that is the case for a 150 cm (5 ft.) antenna cable with the monocycle pulse, shown in Fig. 6.

The semi-log plot of Fig. 6 shows excellent agreement with an exponential fit, as anticipated from the use of the log amp. Because of the reflection coefficients, the calibration data shown for the 150 cm cable in Fig. 6 does not apply to cables of different length, as the MiniPulse utilizes the resonant cavity formed by the cable. Trendlines for 300 and 450 cm cables (10 ft., 15 ft.) are above and to the left of the trendline in Fig. 6, as discussed in [4], thus the system is less sensitive to pulses for longer cables. Another reason for reduced sensitivity could be cable losses at longer length; simpler estimation methods for pulse effects will soon be available [14]. The extreme case of an impedance-matched monocycle source turns out to be unacceptable for the MiniPulse event detector. Fortunately, the 150 cm length is preferred for manufacturing use and conveniently is also our most sensitive example. In general, one must calibrate to the chosen antenna length.

Another consideration in calibration, not covered in [3, 4], is that real antenna signals will not always be as crisp as in Fig. 3; they often look like the bottom of Fig. A3 in Appendix A, from [6]. Imagine the field picked up by the antenna if the dipole collapse was an irregular "shower" of sparks spread over a short period of time, i.e., many dipole collapses. This

often happens and is not unwelcome, because it reduces the worst-case stress. But the effect on triggering of the MiniPulse is not known or well understood. Limited observations, and the electronics as described in [6], suggest that triggering by a signal as in Fig. A3 will happen at a lower worst-case Vp-p. Thus, if Vp-p is our indicator of strong CDM dipole collapse, it is likely that truly hazardous pulses will still not be missed by the MiniPulse box if it is set based on simple calibration curves such as Fig. 6.

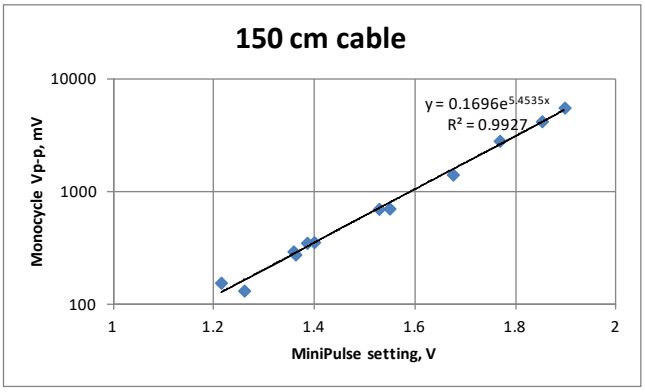


Fig. 6. Monocycle pulse peak-to-peak voltage (Vp-p) magnitude vs. threshold setting of MiniPulse event detector, semi-log plot. Excellent agreement with exponential fit (422 mV/decade).

Along with fragmented dipole collapse, another "wild card" in observation of real CDM in manufacturing is that we don't necessarily know the dipole moment (*dl* in (1)) for an event. But the entire antenna signal scales accordingly, and we have to choose some worst-case value as we decide what Vp-p is dangerous without causing too many false alarms. With higher speeds, component pin length has decreased over time, weakening the likely E-field. Examining the particulars of the device in manufacturing (Fig. A1) is suggested, with attention toward effective dipole length and distance from event to antenna.

Longer term, not only should the MiniPulse box be studied and calibrated better for "real" antenna signals, but improvements and better options for inexpensive detection electronics may be found. If we find, with manual scope measurements, that we wish most of all for strict maximum Vp-p detection at a fast time scale, then it is time to visualize and build a low-cost Vp-p detector. Despite these numerous uncertainties, the treatment in this series of papers of CDM, E and H fields due to dipole collapse, and elements of antenna response should help guide the way.

## V. Conclusions

Charged Device Model ESD [15] is a well-known failure mechanism in semiconductor manufacturing. The fields of a CDM-like pulse can be generated by using an air spark to collapse an electric dipole in a handheld instrument, one that also allows measurement of the current pulse. The E-fields nearby can be picked up and measured by a small "monopole" antenna, whose transfer function can be estimated from antenna dimensions. The result is a measured signal (combining static field, induction field, and radiation field) that is remarkably close to what is predicted from pulsed Hertzian dipole theory [5] from the known parameters, and affords considerable insight into the monitoring of actual CDM events in a semiconductor factory. Because the air spark is hard to control in the instrument and even harder to control in the factory (where we are trying to avoid it!), only the strongest events look just like the theoretical prediction, but those are the worst-case events of highest interest. The antenna waveforms can put definite bounds on the associated CDM event in terms of current and charge quantity, although complete "current imaging" from the antenna signal, as described in [5], remains a difficult goal.

It has been important to recognize the CDM radiation event as being well approximated by the pulsed Hertzian dipole, and as one that benefits from a pole-zero treatment in the s-domain. As described in [5], these tools have largely been overlooked in earlier reviews of pulsed Hertzian dipoles [16], where the tradition has been to use a Gaussian waveform, having no defined t=0, no oscillations, and freedom to choose only the time scale and strength of the pulse. Treatments of pulsed dipole radiation using the Laplace Transform have been rare [5]--one noteworthy case from the late Carl E. Baum, written in 1968, was concerned only with far fields and was not declassified until 1994 [17]. In the present day, the inverse Laplace Transform is so readily available with math software, even as a free applet on the web [18], that the accepted method of acquiring a quick grasp of pulsed fields and signals really ought to change. The monopole antenna transfer function can be worked into the same pole-zero scheme through approximate models [3-5, 12] for such an antenna. This formulation of the field and signal expressions in the s-domain, with Heaviside inversion of the Laplace Transform into the time domain through computer tools, allows a complete and concise picture of the fields to be acquired quickly.

The CDM event as described by dipole collapse is idealized, and is an event we are actually trying to avoid in manufacturing. Thus there are numerous uncertainties and irregularities. Even so, the main feature of a monopole antenna response to a CDM event is a fast bipolar pulse, with peak-peak voltage Vp-p of, usually, tens to hundreds of millivolts. Similar monocycle pulses can be made very reproducibly by augmenting a TLP system with two high-speed directional couplers so that a non-ideal step is (nearly) differentiated twice. This artificial antenna pulse is useful for studying any kind of CDM ESD event detector, e.g., one aimed at replacing the oscilloscope in the factory with a small alarm box attached to the antenna. The CDM event detector studied here [6] showed predictable response to antenna Vp-p over a wide dynamic range. But it may not be the last word in detector design for the semiconductor factory.

## Appendix A

Here we present a few figures from the CDMES patent [6], in support of various discussions in the main text.

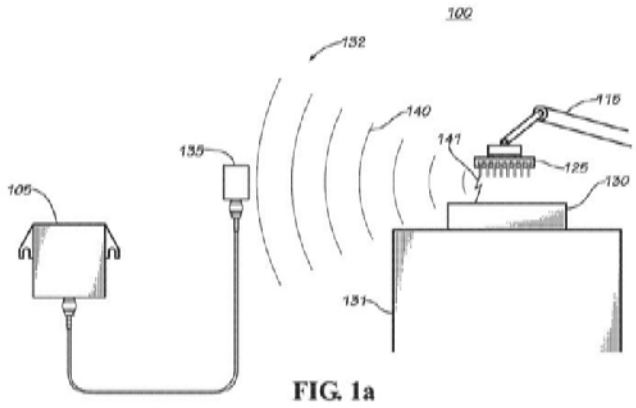


FIG. 1a

Fig. A1. Fig. 1a from [6], ESD detection setup in manufacturing where CDM event from component produces radiation.

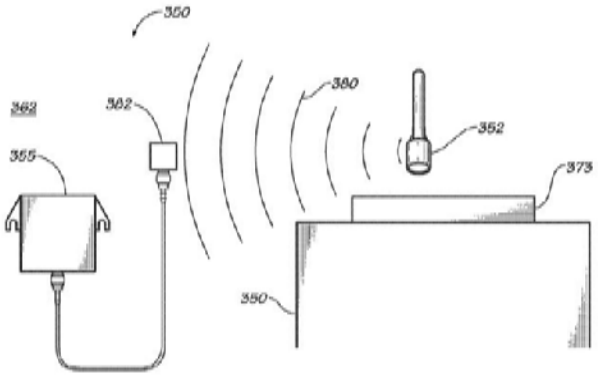


FIG. 3b

Fig. A2. Fig. 3b from [6], with CDMES (CDM Event Simulator) producing CDM radiation in place of component.

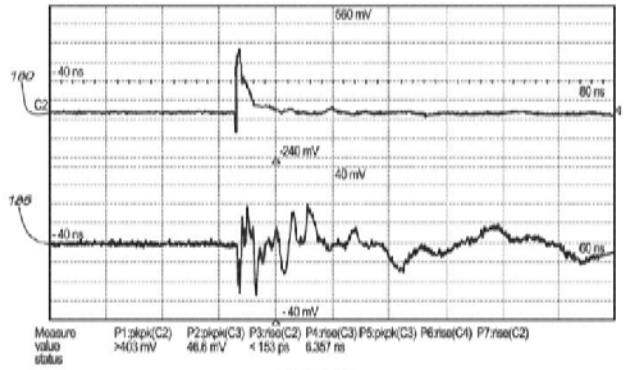


FIG. 1b

Fig. A3. Fig. 1b from [6], CDMES current (top) and antenna signal (bottom) traces.

## ACKNOWLEDGMENT

This work includes much content [1, 3-6, 9-11] from when the author was with Intel Corp. The CDMES was developed mostly from 2010-12 through numerous visits to the co-authors of [6] at Simco-Ion (an ITW company), Emeryville, CA.

## REFERENCES

[1] J. A. Montoya and T.J. Maloney, "Unifying Factory ESD Measurements and Component ESD Stress Testing", 2005 EOS/ESD Symposium, Sept. 2005, pp. 229-237.

[2] A. Jahanzeb, K. Wang, J. Harrop, J Brodsky, T. Ban, S. Ward, J. Schichi, K. Burgess and C. Duvvury, "Capturing Real World ESD Stress with Event Detector", 2011 EOS/ESD Symposium, pp. 197-201.

[3] T.J. Maloney, "Antenna Response to CDM E-fields", 2012 EOS/ESD Symposium, Sept. 2012, pp.269-278.

[4] T.J. Maloney, "Pulsed Hertzian Dipole Radiation and Electrostatic Discharge Events in Manufacturing", IEEE EMC Society Magazine, Q3/2013 issue, pp. 49-57.

[5] T.J. Maloney, "Easy Access to Pulsed Hertzian Dipole Fields Through Pole-Zero Treatment", cover article, IEEE EMC Society Newsletter, Summer 2011, pp. 34-42. See http://ewh.ieee.org/soc/emcs/acstrial/newsletters/summer11/index.html.

[6] Lyle D. Nelsen, Steven B. Heymann, Mark E. Hogsett, and Timothy J. Maloney, Provisional Application, "In-tool ESD Events Monitoring Method and Apparatus", filed with US Patent Office (ITW Ref. 60834-US) Dec. 26, 2013. Issued as US Patent 9,671,448, June 6, 2017 (without TJM, as Intel dropped out during pendency).

[7] S. Ramo, J. Whinnery, and T. Van Duzer, *Fields and Waves in Communication Electronics* (New York: John Wiley & Sons, 1965).

[8] J. D. Jackson, *Classical Electrodynamics*, 3rd Edition (New York: John Wiley and Sons, 1999).

[9] T.J. Maloney and N. Jack, "CDM Tester Properties as Deduced from Waveforms", 2013 EOS/ESD Symposium, Sept. 2013, pp. 374-382. Expanded version in IEEE Trans. Device and Materials Reliability, vol. 14, no. 3, pp. 792-800, Sept. 2014.

[10] T.J. Maloney, "HBM Tester Waveforms, Equivalent Circuits, and Socket Capacitance", 2010 EOS/ESD Symposium, pp. 407-415. See https://sites.google.com/site/esdpubs/documents/esd10.pdf.

[11] T.J. Maloney and A. Daniel, "Filter Models of CDM Measurement Channels and TLP Device Transients", 2011 EOS/ESD Symposium Proceedings, pp. 386-394. See https://sites.google.com/site/esdpubs/documents/esd11.pdf.

[12] S. Caniggia and F. Maradei, "Numerical Prediction and Measurement of ESD Radiated Fields by Free-Space Field Sensors", IEEE Trans. on Electromagnetic Compatibility, vol. 49, no. 3, pp. 494-503 (Aug. 2007).

[13] R.L. Wigington and N.S. Nahman, "Transient Analysis of Coaxial Cables Considering Skin Effect", Proc. IRE, vol. 45, pp. 166-174, Feb. 1957.

[14] T.J. Maloney, "A Turnkey Method for Calculating Coaxial Cable Loss Effects on CDM Waveforms", poster paper submitted to 2018 Electrical Overstress/Electrostatic Discharge Symposium

[15] ANSI/ESDA/JEDEC JS-002-2014, "Charged Device Model (CDM)--Device Level", test standard available at www.esda.org and www.jedec.org.

[16] G. Franceschetti and C.H. Papas, "Pulsed Antennas", IEEE Trans. on Antennas and Propagation, Vol. AP-22, No. 5, Sept. 1974, pp. 651-661. Also is a government report, online at http://www.ece.unm.edu/summa/notes/Sensor.html, SSN 203.

[17] C. E. Baum, SSN 65, "Some Limiting Low-Frequency Characteristics of a Pulse-Radiating Antenna", 28 Oct 68, Air Force Weapons Laboratory. Available online at http://www.ece.unm.edu/summa/notes/SSN/note65.pdf.

[18] Web resource, https://www.symbolab.com/solver/inverse-laplace-calculator.